Journal for ImmunoTherapy of Cancer

Interactions between LAMP3+ dendritic cells and T-cell subpopulations promote immune evasion in papillary thyroid carcinoma

Zhiyuan Wang,[1] Xiaoyu Ji,[1] Ye Zhang,[2] Fan Yang,[1] Hongyue Su,[1] Hao Zhang,[1] Zhendong Li,[3] Wenqian Zhang,[3] Wei Sun [1]

To cite: Wang Z, Ji X, Zhang Y, *et al*. Interactions between LAMP3+ dendritic cells and T-cell subpopulations promote immune evasion in papillary thyroid carcinoma. *Journal for ImmunoTherapy of Cancer* 2024;**12**:e008983. doi:10.1136/jitc-2024-008983

► Additional supplemental material is published online only. To view, please visit the journal online (https://doi.org/10.1136/jitc-2024-008983).

ZW, XJ and YZ contributed equally.

Accepted 13 May 2024

[1]Department of Thyroid Surgery, The First Hospital of China Medical University, Shenyang, Liaoning, People's Republic of China
[2]The First Laboratory of Cancer Institute, The First Hospital of China Medical University, Shenyang, Liaoning, People's Republic of China
[3]Department of Head and Neck Surgery, Cancer Hospital of China Medical University, Shenyang, Liaoning, People's Republic of China

Correspondence to
Wenqian Zhang;
652603034@qq.com

Wei Sun;
Sun19890208@126.com

ABSTRACT

Background The incidence of papillary thyroid cancer (PTC) continues to rise all over the world, 10–15% of the patients have a poor prognosis. Although immunotherapy has been applied in clinical practice, its therapeutic efficacy remains far from satisfactory, necessitating further investigation of the mechanism of PTC immune remodeling and exploration of novel treatment targets.

Methods This study conducted a single-cell RNA sequencing (scRNA-seq) analysis using 18 surgical tissue specimens procured from 14 patients diagnosed with adjacent tissues, non-progressive PTC or progressive PTC. Key findings were authenticated through spatial transcriptomics RNA sequencing, immunohistochemistry, multiplex immunohistochemistry, and an independent bulk RNA-seq data set containing 502 samples.

Results A total of 151,238 individual cells derived from 18 adjacent tissues, non-progressive PTC and progressive PTC specimens underwent scRNA-seq analysis. We found that progressive PTC exhibits the following characteristics: a significant decrease in overall immune cells, enhanced immune evasion of tumor cells, and disrupted antigen presentation function. Moreover, we identified a subpopulation of lysosomal associated membrane protein 3 ($LAMP3^+$) dendritic cells (DCs) exhibiting heightened infiltration in progressive PTC and associated with advanced T stage and poor prognosis of PTC. $LAMP3^+$ DCs promote $CD8^+$ T cells exhaustion (mediated by NECTIN2-TIGIT) and increase infiltration abundance of regulatory T cells (mediated by chemokine (C-C motif) ligand 17 (CCL17)-chemokine (C-C motif) receptor 4 (CCR4)) establishing an immune-suppressive microenvironment. Ultimately, we unveiled that progressive PTC tumor cells facilitate the retention of $LAMP3^+$ DCs within the tumor microenvironment through NECTIN3-NECTIN2 interactions, thereby rendering tumor cells more susceptible to immune evasion.

Conclusion Our findings expound valuable insights into the role of the interaction between $LAMP3^+$ DCs and T-cell subpopulations and offer new and effective ideas and strategies for immunotherapy in patients with progressive PTC.

WHAT IS ALREADY KNOWN ON THIS TOPIC

⇒ Although immunotherapy has been applied in clinical practice, its therapeutic efficacy remains far from satisfactory, necessitating further investigation of the mechanism of papillary thyroid cancer (PTC) immune remodeling and exploration of novel treatment targets.

WHAT THIS STUDY ADDS

⇒ The present results revealed the dynamic nature of the immune microenvironment in the PTC during disease progression from non-progressive PTC to progressive PTC and the specific mechanism by which lysosomal associated membrane protein 3 (LAMP3+) dendritic cells (DCs) mediate immune evasion during PTC clinical progression.

HOW THIS STUDY MIGHT AFFECT RESEARCH, PRACTICE OR POLICY

⇒ Our findings expound valuable insights into the role of the interaction between LAMP3+DCs and T-cell subpopulations and offer new and effective ideas and strategies for immunotherapy in patients with progressive PTC.

INTRODUCTION

The incidence of papillary thyroid cancer (PTC), the most common type of differentiated thyroid cancer (DTC), has increased since the early 1980s, becoming the fastest-growing cancer in most countries, with an increase in incidence of ~5% annually in the USA.[1 2] Most PTCs present an indolent clinical course and can be cured using standard therapeutic strategies, including surgery, radioactive iodine, and thyroid stimulating hormone suppression.[3] However, 10–15% of PTC cases cannot be cured by standard therapy alone and show metastases to distant sites. Patients exhibiting these aggressive forms show a 5-year survival rate of less than 50%.[4] Several scientific advancements have facilitated the elucidation of molecular pathways, such as mitogen-activated protein kinase (MAPK) signaling in thyroid cancer.[5] Multiple kinase inhibitor drugs targeting the

MAPK pathway have shown some clinical benefits but improvements in overall survival remain controversial.[6] Recent efforts and advances in translational research suggest several strategies for immunomodulation in thyroid cancer to restore the functional ability of different immune cells to target neoplastic cells. It includes inhibiting the recruitment of tumor-associated macrophages,[7] identifying tumor-specific antigens to produce tumor vaccines,[8] and blocking and inhibiting immune checkpoints.[9] However, due to the small number of subjects and high incidence of side effects after administration, immunotherapy for thyroid cancer has tremendous scope for improvement in terms of efficacy.[10 11] Novel immunotherapy approaches must be explored for the treatment of progressive thyroid cancers.

The tumor microenvironment (TME) is complex and important in the development, progression, metastasis, and drug resistance of tumors. TME is a key mediator for therapeutic resistance and tumor progression.[12] For example, Severson *et al* found that PD-1$^+$ Tim-3$^+$ CD8$^+$ T lymphocytes exhibited varied degrees of functional exhaustion in patients with regionally metastatic DTC.[13] Zhao *et al* found that M2 polarization of macrophages could induce the formation of a premetastatic niche and promote metastasis of colorectal cancer cells by secreting CXCL13.[14] Multiple cell types collectively form an immunosuppressive TME, promoting tumor immune evasion and reducing the efficacy of single-targeted therapy and immunotherapy. Considering the complexity of the TME, single-cell RNA sequencing (scRNA-seq) analysis, with comprehensive transcriptomics profiling at single-cell resolution and an unbiased catalog of cellular diversity, is a promising tool to extensively investigate the immune heterogeneity in the TME.

As the most potent antigen-presenting cells, dendritic cells (DCs) enhance their antigen-presenting effect on tumor cells and the activation of effector T cells. However, in recent years, the carcinogenesis of DCs has been discussed and verified using scRNA-seq analysis. Zhang *et al* showed that lysosomal associated membrane protein 3 (LAMP3$^+$) () DCs in tumors metastasizing to the lymph nodes may be likely to recruit and activate regulatory T cells (Tregs) to enhance immunosuppression.[15] Peng *et al* found that enrichment of M2-polarized macrophages and LAMP3+DCs conferred enhanced immune suppression in recurrent nasopharyngeal carcinoma.[16] However, the role of LAMP3$^+$ DCs in immune evasion and progression to advanced PTC is not clear.

This study attempted to investigate the genetic changes occurring during the progression of PTC at the single-cell level using scRNA-seq analysis of 4 para-carcinoma tissues, 4 non-progressive PTC cases and 10 progressive PTC cases. Cases of progressive PTC exhibited immune evasion and identified a cluster of LAMP3$^+$ DCs involved in immune tolerance. These LAMP3$^+$ DCs played a dual role. On the one hand, they attracted CD8$^+$ T cells and induced CD8$^+$ T-cell exhaustion through several ligand-receptor interactions such as NECTIN2-TIGIT; on the other hand, they recruited Treg cells into tumor foci through multiple chemotactic factors such as chemokine (C-C motif) ligand 17 (CCL17)-chemokine (C-C motif) receptor 4 (CCR4) signaling and promoted immune evasion in PTC, ultimately leading to clinical progression. Our findings elucidated the potential mechanisms of immune evasion in PTC and provided a theoretical basis for further studies.

METHODS

Human specimens

14 patients who underwent surgery at the First Hospital of China Medical University were enrolled in our study. A total of 18 fresh surgical specimens were sequenced and incorporated in subsequent analyses. Four of these specimens were non-progressive PTCs with a follow-up period exceeding 5 years, during which no clinical progression was observed. 10 specimens were PTCs that exhibited clinical progression, including tumor enlargement (N=9), lymph node metastasis (LNM) (N=10), extrathyroidal extension (ETE) (N=6) or distant metastasis (N=3). The remaining four specimens are adjacent tissues from one case of non-progressive PTC and three cases of progressive PTC, respectively. Spatial transcriptomics sequencing was performed using paraffin sections of 2 patient tumors from 14 patients (a non-progressive PTC vs a progressive PTC). Two experienced pathologists carefully reviewed the H&E-stained sections of each sample to confirm the pathology. Online supplemental table S1 provides a summary of the clinical information, including demographics, tumor clinicopathologic characteristics, and treatment history.

Tissue dissociation and preparation of single-cell suspensions

Fresh tissue samples were excised and subjected to two washes with 1× phosphate-buffered saline (PBS). Subsequently, the tissue was transferred to a sterile RNase-free culture dish on ice, which contained the appropriate amount of calcium-free and magnesium-free 1× PBS. The tissue was then transferred to a culture dish and cut into pieces measuring 0.5 mm^2. Subsequently, it was washed with 1× PBS while ensuring the careful removal of any non-essential tissues, such as blood stains and fatty layers.

The tissues were dissociated into individual cells by treating them with a dissociation solution composed of 0.2% collagenase II, 2 mg/mL papain, and 120 units/mL DNase I. The mixture was then incubated in a water bath set at 37°C with gentle shaking for 20 min at 100 rpm. The digestion process was stopped by adding 1× PBS containing 10% fetal bovine serum (V/V) and gently pipetting the solution 5–10 times using a Pasteur pipette. The resulting cell suspension was filtered using a 70–30 µm stacked cell strainer and then centrifuged at 300 g for 5 min at 4°C. The obtained cell pellet was then resuspended in 100 µL of 1× PBS containing 0.04% bovine serum albumin (BSA) and mixed with 1 mL of 1× red blood cell lysis buffer (MACS 130-094-183, 10×). The mixture was incubated

at room temperature or on ice for 2–10 min to facilitate lysis of any remaining red blood cells. Following incubation, the suspension was centrifuged at 300 g for 5 min at room temperature. The resulting suspension was then mixed with 100 µL of Dead Cell Removal MicroBeads (MACS 130-090-101) and dead cells were removed using the Miltenyi Dead Cell Removal Kit (MACS 130-090-101). The suspension was subsequently resuspended in 1× PBS containing 0.04% BSA and repeated centrifugations at 300 g for 3 min at 4°C were performed (twice). The resulting cell pellet was resuspended in 50 µL of 1× PBS containing 0.04% BSA. The viability of cells, required to be above 85%, was confirmed using trypan blue exclusion, and the single-cell suspensions were counted with a Countess II Automated Cell Counter. The concentration was then adjusted to a range of 700–1,200 cells/µL.

Single-cell RNA-seq and reads processing

Individual cells in single-cell suspensions were captured by loading them onto the 10x Chromium system, following the manufacturer's instructions for the 10x Genomics Chromium Single-Cell 3' kit (V.3). Following standard protocols, the subsequent steps involved amplifying the complementary DNA (cDNA) and constructing libraries. LC-Bio Technology performed paired-end sequencing (150 nt) on Illumina NovaSeq 6000 Systems to sequence the libraries, which contained the single-cell data. The Cell Ranger toolkit (V.3.1) was used to generate gene-barcode matrices. Using the droplet-based sequencing data, this toolkit aligned the data to the Genome Reference Consortium human genome assembly build 38 human reference genome and counted the unique molecular identifiers (UMIs) for each cell.

Quality control and batch effect correction of scRNA-seq data

For quality control procedures and downstream bioinformatic analyses, we primarily used the "Seurat" R package (V.4.2.0). Initially, we filtered out cells with low quality based on specific criteria. Cells with less than 2,001 UMIs, more than 6,000 or less than 201 expressed genes, or with more than 10% UMIs derived from the mitochondrial genome were excluded. We employed the "DoubletFinder" package (V.2.4) with default settings to identify and remove potential doublets. After completing the quality control procedures, we performed a series of preprocessing techniques for downstream analysis. We applied global-scaling normalization using the "LogNormalize" method, which normalized the feature expression for each cell based on total expression and scaled it by a default factor of 10,000. The resulting expression values were then log-transformed using the "NormalizeData()" function in Seurat. Subsequently, we merged the normalized expression profiles from all samples using the "merge()" function in R V.4.1.3. The "harmony" package (V.0.1.0) addressed batch effects. Batch effect correction was performed using the top 5,000 highly variable genes (HVGs) identified by the FindVariableFeatures() function from the merged data set. Finally, we obtained scaled and batch effect-corrected expression profiles of all samples for downstream analyses.

Unsupervised clustering and dimensional reduction

After performing batch effect correction, we computed the top principal components (PCs) using the gene expression profiles of the top 5,000 HVGs. To determine the optimal number of PCs for further analysis, we used the PCElbowPlot() function in Seurat as recommended in V.4.2.0. For cell clustering, we applied the FindNeighbors() and FindClusters() functions in Seurat. To obtain appropriate visualizations, we used the RunTSNE() and RunUMAP() functions. We defined cell identities within each cluster based on the expression of known marker genes, and assigned the cell identity of each cluster based on the expression of established marker genes. In the first round of "low-resolution" clustering, we identified myeloid cells (CSF1R, FCER1G, LYZ), T and NK cells (CD3D, IL-7R, NKG7), B cells/plasma cells (CD79A, MS4A1, IGKC, JCHAIN), progenitor cells (MKI67, STMN1), thyroid epithelial cells (thyrocyte, TG, EPCAM, KRT19), fibroblasts (RGS5, DCN, COL1A1, ACTA2), and endothelial cells (RAMP2, VWF, FLT1). We subsequently conducted the second round of "high-resolution" clustering to identify the finer subclusters within each significant cell type.

Identification of signature genes for cell clusters

We employed the FindAllMarkers() function in Seurat to identify differentially expressed genes (DEGs) within each subcluster. The significance of these genes was assessed using the Wilcoxon rank-sum test with Bonferroni correction. Selection of signature genes was based on the following criteria: (1) expressed in >20% of cells in either or both groups, (2) |log2FC|>0.5, and (3) adjusted p value<0.05 for the Wilcoxon rank-sum test.

Pathway analysis

We used the Gene Set Variation Analysis (GSVA) R package (V.1.42.0) to perform GSVA and estimate the enrichment scores of biological pathways. The hallmark and Gene Ontology (GO) gene sets were obtained from the msigdbr R package (V.7.5.1) and the MsigDB website (http://software.broadin-stitute.org/gsea/msigdb). To evaluate the differential activities of pathways between different clusters or groups, we employed the limma R package with a significance threshold of p<0.05.

Cell–cell communication analysis

To evaluate interaction numbers and strength and investigate potential communication between different cell types based on the expression of ligand-receptor pairs, we employed the "CellChat" package (V.1.5.0) with default parameters. The inclusion of a receptor or ligand in the downstream analysis required expression in more than 10% of cells within a cluster. Empirical p values were calculated by randomly assigning cluster labels 1,000 times for each cell pair to determine the significance of a ligand-receptor pair between two clusters.

Spatial transcriptomics sequencing

Following resection, samples were gathered and subjected to a tissue optimization experiment using the 10x Genomics Visium Spatial Tissue Optimization (Rev A) platform. Initially, tissue staining and imaging protocols were executed, followed by tissue permeabilization and fluorescent cDNA synthesis, with RNA quality assessment (RNA integrity number >7.0). Subsequent to tissue removal, slide imaging was conducted. We then proceeded to perform Visium Spatial Gene Expression analysis employing the 10x Genomics Visium Spatial Gene-Expression Reagent Kits (Rev B). Initially, tissues were fixed and stained for imaging, followed by tissue permeabilization at varying durations (3, 6, 12, 18, 24, and 30 min). Notably, a 12 min permeabilization period resulted in the highest fluorescence signal in both tumor and adjacent normal regions of the thyroid. This was succeeded by reverse transcription, second-strand synthesis, denaturation, cDNA amplification, quality control, Visium Spatial Gene-Expression library construction, and ST sequencing, following the manufacturer's instructions. These procedures yielded data sets comprising 4,429 (SPT-A1) and 4,895 (SPT-B7) spots. Subsequent analysis is the same as single-cell sequencing analysis.

Flow cytometry

Single-cell suspensions were prepared using the methods described above. For flow cytometry, cells were stained in fluorescence-activated cell sorting (FACS) buffer containing PBS supplemented with 2% BSA and 5 mM EDTA. Monoclonal antibodies specific to CD45 (FITC, BioLegend, Cat# 982316), HLA-DR (PerCP-Cy5.5, BioLegend, Cat#307629), CD11c (Pacific Blue, BioLegend, Cat#301627), CD1c (APC, BioLegend, Cat#331523), DC_LAMP/CD208 (APC, Invitrogen, Cat# 17-2089-41), CD80 (PE, BioLegend, Cat#305207), IL-12/IL-23 p40 (PE, Invitrogen, Cat#501806) were used for this purpose. For intracellular staining, cells were fixed with Invitrogen Fix/Perm, following the instructions provided in the kit, for intracellular cytokine stains.

Immunohistochemistry and multiplex immunohistochemistry staining assay

We obtained fresh 48 non-progressive PTC and 53 progressive PTC tissues from patients. Immunohistochemistry for the target molecules was performed on paraffin sections using a primary antibody recognizing TIGIT (1:1,000, Cell Signaling Technology, Cat#99567T), FOXP3 (1:2,000, Abcam, Cat#ab215206), or LAMP3/CD208 (1:400, CST, Cat#47778). 10 pairs of formalin-fixed, paraffin-embedded tissue sections were processed for multiplex immunohistochemistry (mIHC) staining assay using the mIHC/immunofluorescence staining kits (Absin, Shanghai, China, Cat#abs50014) according to the manufacturer's instructions. The following antibodies were used in the current study: primary antibodies against DC_LAMP/CD208 (1:400, CST, Cat#47778), CD8A (1:100 dilution; Abcam, Cat#ab217344), TIGIT (1:1,000, Cell Signaling Technology, Cat#99567T), NECTIN2 (1:400, Cell Signaling Technology, Cat#95333T), NECTIN3 (1:500, R&D, Cat#AF3064-SP), CCL17 (1:1,000, Abcam, Cat#ab195044), KRT19 (1:2,000, Abcam, Cat#ab76539), FOXP3 (1:2,000, Abcam, Cat#ab215206), or CCR4 (1:2,000, Novus Biologicals, Cat#NBP1-86584). The fluorescent signals were photo-imaged and merged using a laser scanning confocal microscope (ZEISS, LSM880) and inForm software (V.2.42).

RESULTS

Dynamics of the ecosystem in adjacent tissues, non-progressive PTC and progressive PTC

To comprehensively understand the heterogeneity of thyroid cancer at the single-cell level, we collected 18 (4 adjacent normal tissues, 4 non-progressive PTCs and 10 progressive PTCs) tissue samples from 14 patients (online supplemental table S1) and performed scRNA-seq. We further validated our single-cell analysis results using two examples of spatial transcriptomics RNA sequencing (a non-progressive PTC and a progressive PTC), bulk sequencing data from 502 PTC samples from The Cancer Genome Atlas (TCGA) and their corresponding clinical data, immunohistochemistry and mIHC (figure 1A). These 18 tissue samples were categorized into three groups: Normal, Group A and Group B. Normal included four adjacent tissues. Group A encompassed four non-progressive PTCs, while Group B comprised 10 PTCs that had exhibited at least one clinical progression, such as tumor enlargement, LNM, ETE, or distant metastasis (figure 1B). After rigorous quality control measures, we obtained a total of 151,238 cells. Following the elimination of batch effects (figure 1C), these cells were clustered into 23 subgroups through dimensionality reduction using Uniform Manifold Approximation and Projection (UMAP), a non-linear technique (online supplemental figure S1A). Using widely recognized markers, the cells were annotated into seven types, including thyroid follicular epithelial cells (also known as thyrocytes), endothelial cells, fibroblasts, T or natural killer (NK) cells, B cells, myeloid cells, and progenitor cells (figure 1D,E, online supplemental figure S1B–I). The composition of the seven cell types exhibited significant variability among different type samples, highlighting the heterogeneity within normal thyroid tissues and PTC tumors (figure 1B,F, online supplemental figure S1G). Fibroblasts only account for 5% of normal tissues, while they significantly increase to 14% and 19% in non-progressive PTC and progressive PTC, respectively, indicating the presence of richer stroma in tumors, which can construct a more favorable environment for tumor growth. In terms of immune cells, there was no difference in the proportion of total immune cells between normal samples and non-progressive PTC microenvironment, while the proportion of immune cells in progressive PTC decreased significantly. More specifically, the infiltration of B cells

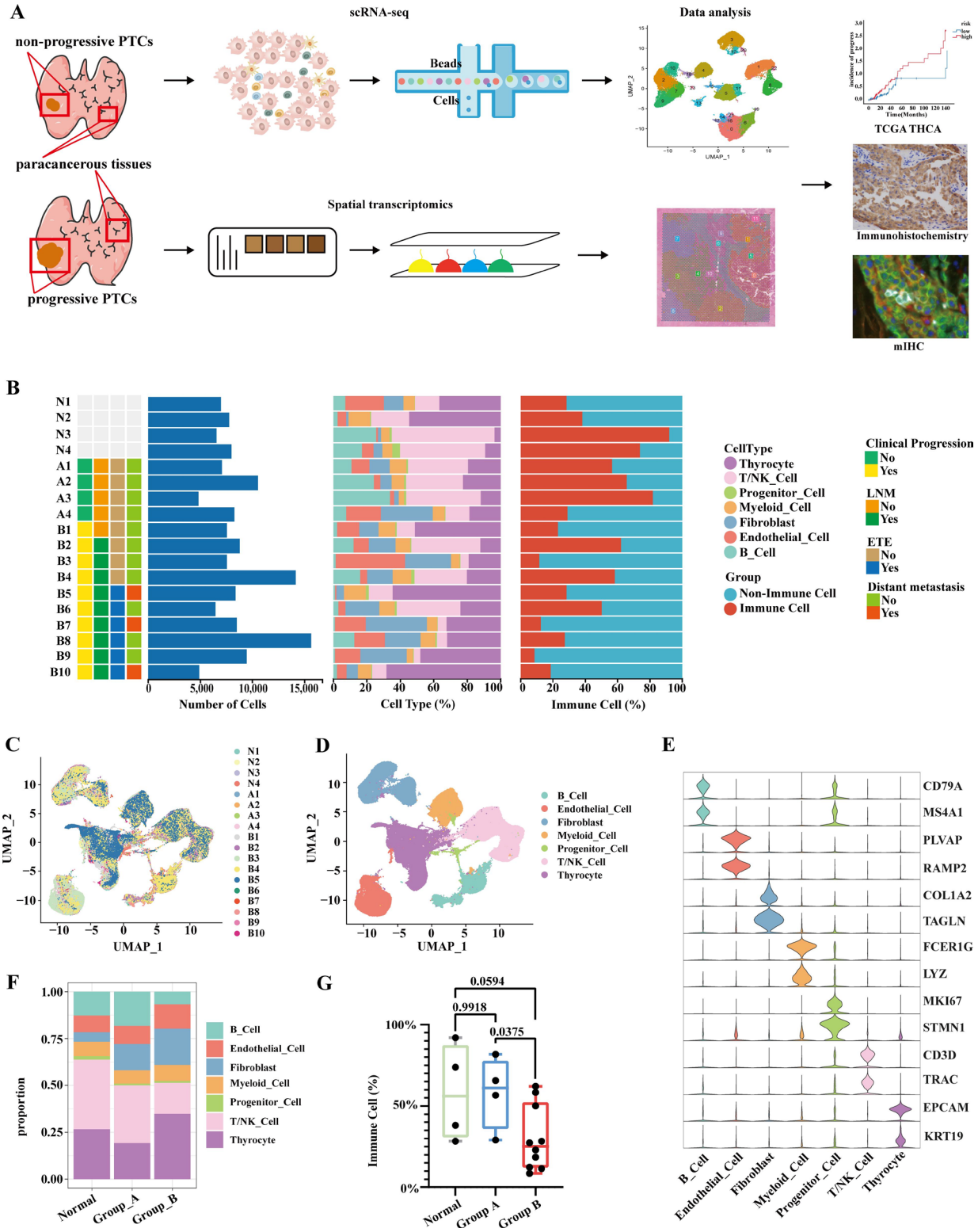

Figure 1 Dynamics of the ecosystem in adjacent tissues, non-progressive PTC and progressive PTC. (A) Overview of the study design and workflow. Single-cell suspensions were collected from 4 adjacent tissues, 4 non-progressive PTC and 10 progressive PTC followed by single-cell transcriptomic sequencing on the 10x Genomics platform. Two paraffin-embedded sample sections for spatial transcriptome sequencing. (B) Clinical features of the patients and the composition of cells in the tumor samples. UMAP of all cells post-quality control and filtering grouped by the sample (C) and major cell type (D). (E) Violin plots showed the distribution of expression levels of canonical cell type markers. (F) Bar plots indicate the proportion of major cell lineages in three groups. (G) Fractions of immune cells in three groups. ETE, extrathyroidal extension; LNM, lymph node metastasis; mIHC, multiplex immunohistochemistry; NK, natural killer; PTC, papillary thyroid cancer; scRNA-seq, single-cell RNA sequencing; TCGA, The Cancer Genome Atlas; THCA, Thyroid carcinoma; UMAP, Uniform Manifold Approximation and Projection.

and T/NK cells was significantly reduced, suggesting that the role of antitumor immunity may be weaker in progressive PTC (figure 1F,G, online supplemental figure S1G). Cell cycle analysis indicated that almost all progenitor cells were in the G2M phase, signifying active proliferation. In contrast, the remaining cell types were evenly distributed across the three cell cycle phases, indicating that the cell cycle did not introduce bias into the overall dimensionality reduction clustering results (online supplemental figure S1K,L). These findings suggest that PTC with clinical progression exhibit higher tumor purity and a TME characterized by reduced immune activity than those without progression.

Thyrocytes of progressive PTC exhibit significant immune evasion

We extracted thyrocytes from the entire population for more refined dimensionality reduction clustering to assess the differential transcriptomic expression patterns of thyroid tumor cells during the clinical progression of PTC. Thyrocytes can be characterized into 10 clusters, evident in cluster distributions in the UMAP plot (figure 2A). By identification of DEGs, we compared the similarities and differences among the clusters and reannotated them into six clusters of thyrocytes (figure 2B). These six clusters showed substantial disparities between samples of the normal group and Group A and Group B. C2_TFF3, with high expression of marker genes of normal thyroid follicular epithelium, including TFF3, TPO, TG, predominant in para-cancerous tissues (up to 80%) (figure 2C). On the contrary, the proportion of C1, C3, C4, and C6 in tumor tissues increased significantly, especially those of C1 and C3 thyrocytes, which increased with tumor progression. Differential genes expressed in these two types of thyrocytes, such as APOE and FN1, were significantly associated with the progression of thyroid cancer (figure 2D). We identified a type of thyrocyte, C6_S100A2, almost exclusively in the progression of PTC. The transcriptional profile of C6_S100A2 differs significantly from other clusters of thyrocytes. We speculated that this cluster may be a marker of clinical progression in PTC. GO functional enrichment analysis showed that C1_APOE, C3_FN1, and C6_S100A2, dominant in PTC tumors, were involved in many biological processes related to immune regulation, such as leukocyte activation and DC migration. C2_TFF3, representing normal thyrocytes, is involved in several metabolic processes and shows little interaction with other cell types in the TME (figure 2E,F, online supplemental figure S2A–D).

We conducted a pseudotime analysis to investigate the evolution of various clusters of thyrocytes. If normal thyrocytes (C2_TFF3) were used as the root, thyrocytes showed a complex evolution and not a simple linear evolution. Among them, C3_FN1, C4_HSPA1A, and C6_S100A2 were found in a relatively late stage of differentiation, indicating that these clusters deviated the farthest from normal thyrocytes and may be more relevant to the clinical progression of PTC (figure 2G,I, online supplemental figure S2E). We used gene signatures associated with thyroid differentiation (three times a day), epithelial-mesenchymal transition (EMT), and immune evasion to score the thyrocytes (figure 2J–L, online supplemental figure S2F,G). Consistent with the results of the pseudotime analysis, the violin plot showed that C2_TFF3 had a higher three times a day score distinct from other clusters of thyrocytes, confirming that C2_TFF3 was well differentiated normal thyroid follicular epithelial cells. Moreover, C3_FN1, C4_HSPA1A, and C6_S100A2 exhibited low three times a day scores to varying degrees, particularly showing significant de-differentiation in C6_S100A2, which typically represents robust malignancy. C6_S100A2 showed the highest EMT score, confirming its enhancing effect on the progression of PTC. In terms of immune evasion scores, thyrocytes in Group B showed higher evasion scores (figure 2L). We compared thyrocytes to determine whether malignant thyrocytes evade recognition and eradication by the immune system through mechanisms such as the upregulation of ligands for well-known immune checkpoints, antigen modulation, or defects in the antigen-processing machinery. Although only a small number of thyrocytes expressed immune checkpoint-related genes, most cells also did not express tumor-associated antigen-related adhesion molecules. Compared with normal cells (C2_TFF3), cells with a dominant role in cancer, such as C1_APOE and C3_FN1 expressed fewer antigen-processing-related genes (figure 2M–O, online supplemental figure S2H–J).

Taken together, these findings highlight significant differences in gene expression and functional activation between adjacent tissues, non-progressive PTC, and progressive PTC thyrocytes. Although the thyrocytes did not show extensive upregulation of ligand expression related to immune checkpoints, thyrocytes that were dominant in tumors and increased with PTC progression showed a general defect in antigen presentation, suggesting significant immune evasion in progressive PTC.

$CD8^+$ T-cell exhaustion and Treg infiltration are higher in progressive PTC

T cells are pivotal in orchestrating antitumor immune responses. They are significant regulators of immune suppression. Various T-cell subtypes perform distinct functions in the immune system. We performed unsupervised T and NK cell clustering analysis for Groups A and B, resulting in the identification of 11 subclusters, including 5 $CD4^+$ T cells, 4 $CD8^+$ T cells, and 2 NK cells (figure 3A). One cluster of $CD4^+$ T cells showed low expression of CD4 and high expression of markers, including chemokine receptor 7 (CCR7), selectin L (SELL), and nuclear receptor subfamily 4 group A member 1, typically associated with naïve T cells[17] (figure 3A,B, online supplemental figure S3A). Another cluster was identified as Treg cells due to its high CTLA-4, FOXP3, IL-2RA, TIGIT, and TNFRSF18 expression levels.[18] The upregulation of markers, including SELL

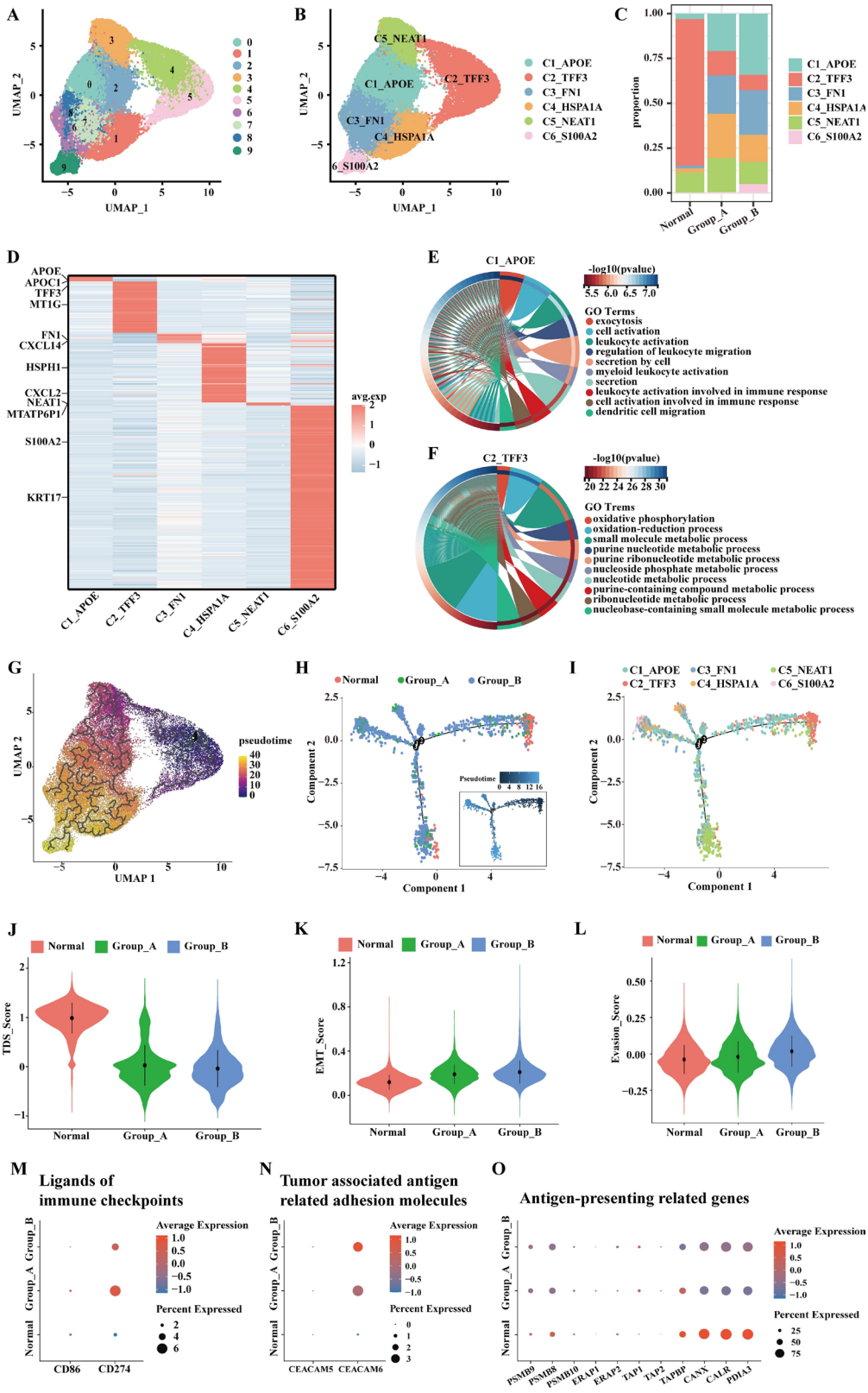

Figure 2 Progressive PTC cells exhibit significant immune evasion. UMAP plot demonstrating 10 clusters based on unsupervised clustering (A) and 6 distinct clusters based on gene expression differences (B) for thyrocytes passing quality control. (C) Bar plots indicate the proportion of six cell lineages in three groups. (D) Heatmap showing differentially expressive genes in six clusters. (E–F) Circle plots show the GO functional differences between the two clusters of thyrocytes. (G–I) Differentiation trajectory of thyrocyte subclusters predicted by Monocle3 and Monocle2. Violin plots showed the three times a day score (J) EMT score (K) and evasion score (L) of different clusters of thyrocytes. (M–O) The dot plots displayed the expression of genes related to immune activity in different clusters of thyrocytes. EMT, epithelial-mesenchymal transition; GO, Gene Ontology; PTC, papillary thyroid cancer; UMAP, Uniform Manifold Approximation and Projection.

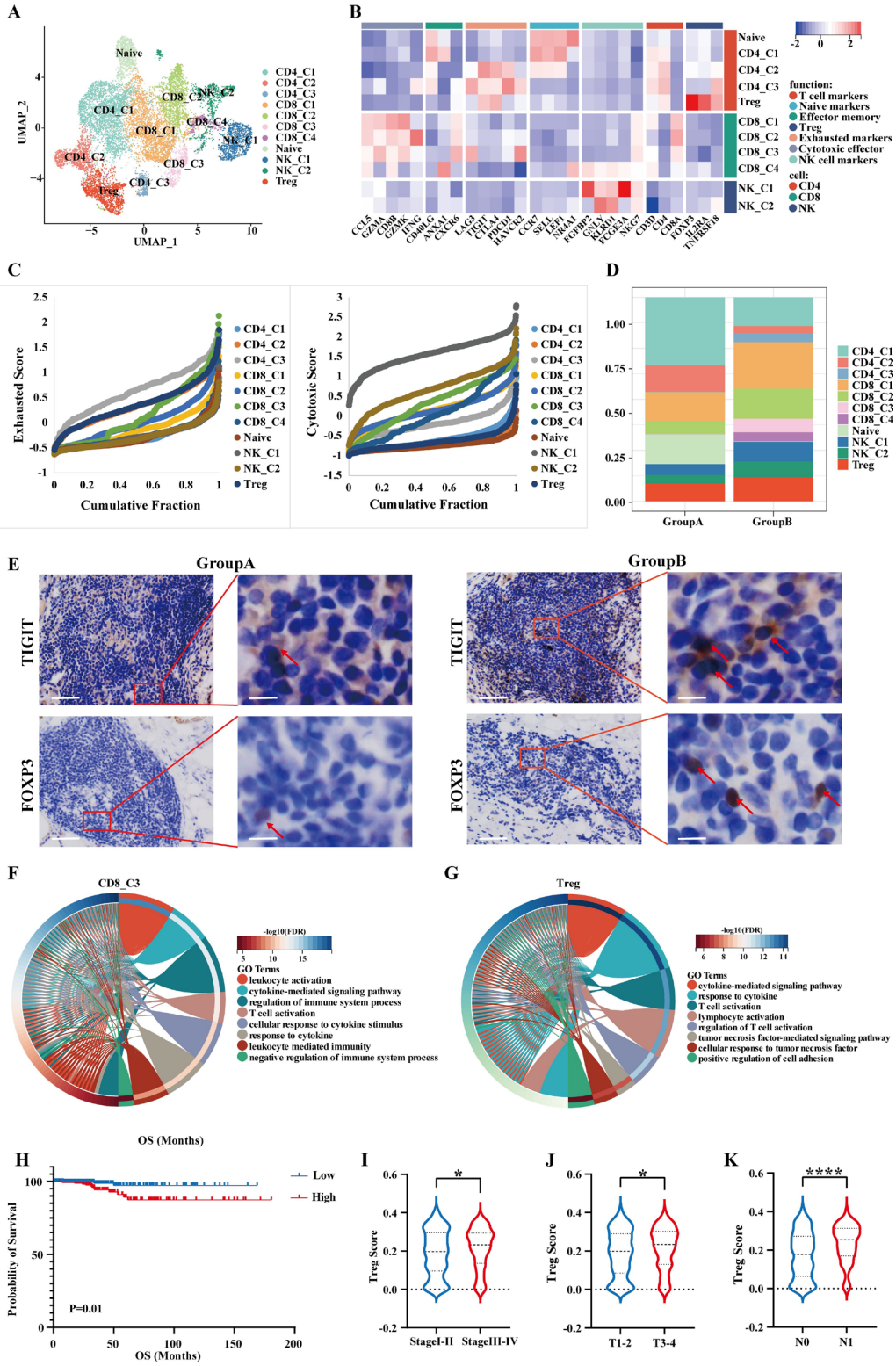

Figure 3 CD8⁺ T-cell exhaustion and Treg infiltration are higher in progressive PTC. (A) UMAP plot demonstrating 11 distinct clusters based on gene expression differences for T/NK cells. (B) Heatmap indicating the expression of selected functionally relevant genes in the T/NK subtypes. (C) Cumulative distribution function showing the distribution of exhausted, cytotoxic, and naïve state scores in each T/NK subtype. A rightward shift of the curve indicates increased state scores. (D) Bar plots indicate the proportion of T/NK subtypes in two groups. (E) Immunohistochemistry revealed differences in TIGIT and FOXP3 expression between two groups (200 µm and 50 µm). Circle plots show the GO functions of CD8_C3 (F) and Treg cells (G). Samples with high exhaustion scores have a poorer prognosis (H) and later clinical stages in the TCGA-THCA cohort (I–K). Samples with high Treg scores have a poorer prognosis (L) and later clinical stages in the TCGA-THCA cohort (M–O). GO, gene ontology; NK, natural killer; OS, overall survival; PTC, papillary thyroid cancer; TCGA, The Cancer Genome Atlas; THCA, thyroid carcinoma; FDR, false discovery rate; Treg, regulatory T cell; UMAP, uniform manifold approximation and projection.

in the CD4_C1 cluster and CD40 ligand, annexin A1, and other activation markers, indicated that these cells were transitioning from an immature to effector T-cell state. Conversely, CD4_C2 and CD4_C3 showed upregulation of TIGIT, CTLA-4, and other markers associated with T-cell exhaustion, suggesting that these clusters of $CD4^+$ T cells were exhausted, characterized by the loss of corresponding cellular functions.[19] Among $CD8^+$ T cells, clusters 1 and 2 (CD8_C1 and CD8_C2) exhibited high expression of cytotoxic genes, including GZMK, GZMA, and NKG7, suggesting that these cells are precursors of cytotoxic T cells.[20] Interferon gamma is significantly overexpressed in CD8_C2 compared with CD8_C1 (figure 3B, online supplemental figure S3B,C). Cluster 3 (CD8_C3) of $CD8^+$ T cells showed high expression of cytotoxicity-related genes (GZMA, NKG7, and GZMK) and exhaustion-related markers (PDCD1, HAVCR2, and LAG3), indicating $CD8^+$ T-cell exhaustion. The CD8_C4 cluster showed high expression of CD8 and NK cell markers (GNLY, FGFBP2, and KLRD1), suggesting that this cluster may represent NK T cells. We constructed a signature using T-cell exhaustion-related genes. CD8_C3 exhibited a higher exhaustion score compared with other CD8 clusters (figure 3C, online supplemental figure S3D–F). The exhausted $CD8^+$ T-cell population (CD8_C3) and Treg cells showed significant enrichment in Group B, indicating enhanced immune exhaustion, immune suppression, and T-cell dysfunction in the TME during clinical progression (figure 3D). We validated the T-cell exhaustion status and Treg infiltration in tissue specimens in non-progressive PTC (N=48) and progressive PTC (N=53) samples through immunohistochemistry (figure 3E). As shown in figure 3F, genes specifically expressed in CD8_C3 were associated with leukocyte activation, cytokine-mediated signaling pathways, and negative regulation of immune system processes. In contrast, Treg cells expressed genes involved in tumor necrosis factor-mediated signaling, cellular responses to tumor necrosis factor, and positive regulation of cell adhesion, culminating in the formation of an immunosuppressive microenvironment which is conducive to tumor growth during clinical progression of PTC (figure 3F,G). These findings suggest a correlation between clinical progression, T-cell exhaustion, and immunosuppressive effects of Treg infiltration. Concerning Treg infiltration, TCGA data indicates that higher Treg infiltration is associated with worse overall survival, and there is an increased presence of Treg infiltration in cases with LNM (figure 3H–K). Similarly, higher exhaustion scores were correlated with worse clinical outcomes and tumor, node, metastases (TNM) staging (online supplemental figure S3G–I). Our findings suggested that $CD8^+$ T cells exhibit higher exhaustion levels in progressive PTC, and their coexistence with increased Treg infiltration indicated a weakening of immune surveillance in progressive PTC.

$LAMP3^+$ DCs enriched in progressive PTC and associated with poor prognosis

Subsequently, we characterized myeloid cells, given the significant upregulation of myeloid leukocyte activation and DC migration regulation observed in tumor thyrocytes. Recognizing that DCs are potent antigen-presenting cells and considering the upregulation of DC chemotaxis-related functions in progressive PTC cells, we focused our research on DCs. A total of 4,865 myeloid cells were identified and classified into seven subsets, which consisted of macrophage cells (labeled by APOE and C1QC), monocyte cells (designated by FCN1 and S100A8), neutrophil cells (indicated by G0S2), and four subsets for DCs (figure 4A, online supplemental files 1, 5 and 8). One DC cluster was identified as $CD141^-CD1C^-$ DC due to the expression of some key genes known to be associated with monocytes.[21] The other three DC clusters have been classified as conventional DC (cDC) based on characteristic gene expression patterns (figure 4B). Among these cDC clusters, cDC_C1 demonstrated high expression of classical conventional dendritic cells type 1 (cDC1) markers, such as C-type lectin domain family 9 member A and X-C motif chemokine receptor 1. cDC1s are critical for generating antitumor immune responses, as they could cross-present tumor antigens derived from necrotic and apoptotic tumor cells.[22 23] In contrast, cDC_C2 exhibited high expression of classical conventional dendritic cells type 2 (cDC2) markers, including CD1C and CD1A. We identified a cluster of $LAMP3^+$ DCs, referred to as cDC_C3 cells, in PTC. These $LAMP3^+$ DCs were characterized by high levels of maturity, activation, and migratory properties, as indicated by the expression of signature genes associated with maturation (UBD and IDO1), activation (CD80, CD83, and CD40), and migration (CCR7 and FSCN1).[24 25] Additionally, $LAMP3^+$ DCs exhibited elevated expression of specific chemokine ligands (CCL17, CCL19, and CCL22) that are known to recruit T cells expressing chemokine receptors, such as CCR4, CCR7, and C-X-C motif chemokine receptor 3 (CXCR3) (figure 4B).[26–29] Furthermore, the infiltration of $LAMP3^+$ DCs was more prevalent in progressive PTC (figure 4C). Based on previous research, we have compiled a list of genes associated with promoting T-cell exhaustion or recruiting Treg cells.[30–36] We have generated gene signatures using these genes and determined that $LAMP3^+$ DCs are the most proficient at promoting T-cell exhaustion and inducing the chemotaxis of Treg cells (figure 4D,E).

Enrichment analyses of GO and Kyoto Encyclopedia of Genes and Genomes (KEGG) signaling pathways revealed distinct patterns among the three cDCs clusters. Specifically, "positive regulation of T helper-2 cell cytokine production" was significantly upregulated in cDC_C1, "positive regulation of chemokine production" was substantially upregulated in cDC_C2 and "negative regulation of immune response" was considerably upregulated in $LAMP3^+$ DCs (online supplemental figure S4D–F). Furthermore, GSVA analysis showed that

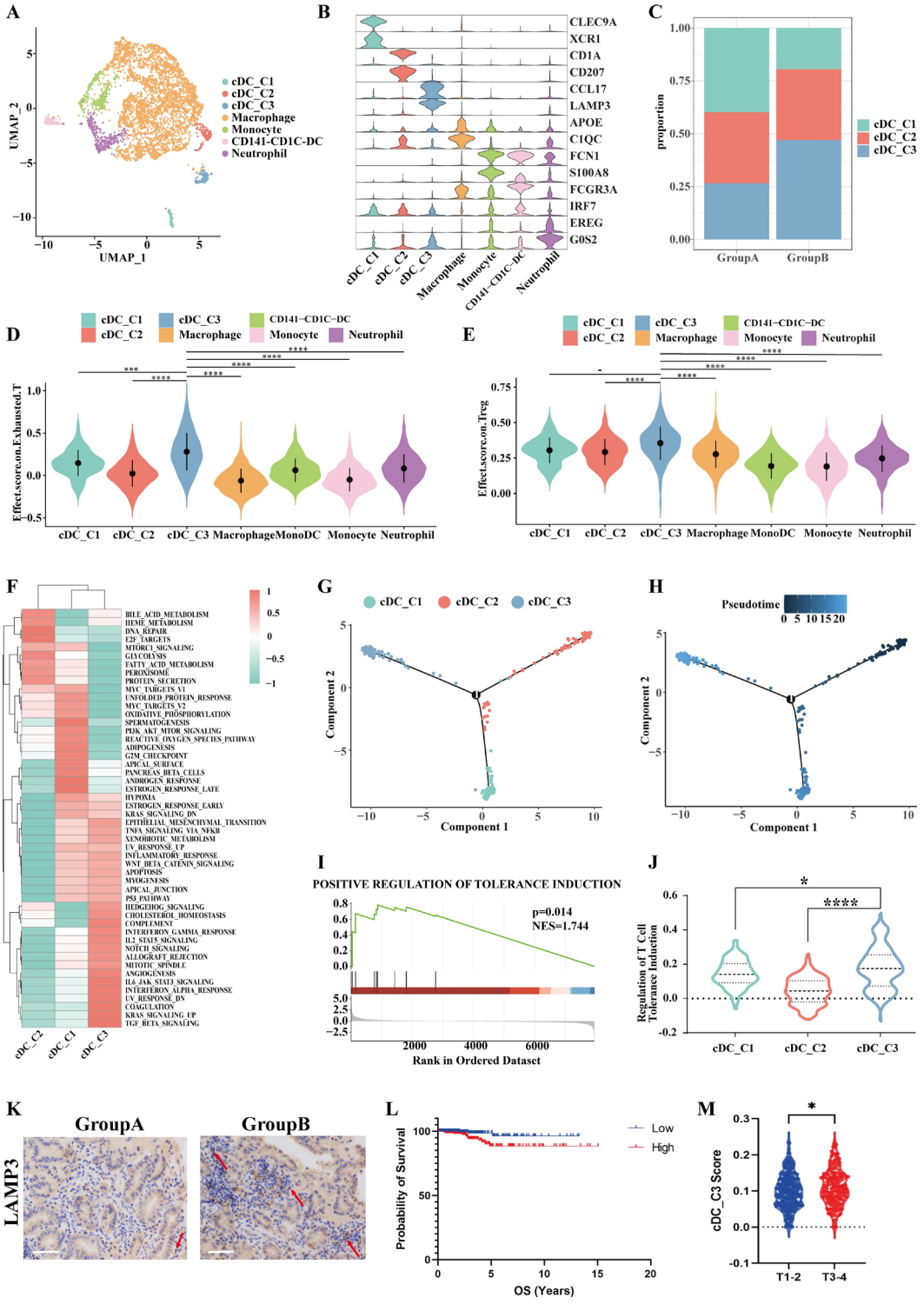

Figure 4 LAMP3⁺ DCs (cDC_C3) enriched in progressive papillary thyroid cancer and associated with poor prognosis. (A) UMAP plot demonstrating seven distinct clusters based on gene expression differences for myeloid cells. (B) Violin plots showing the distribution of expression levels of cell markers of seven myeloid subclusters. (C) Bar plots indicate the proportion of DC subtypes in two groups. Violin plots showing cDC_ C3 has a higher ability to cause T-cell exhausted (D) and recruit Treg cells (E). (F) Heatmap showed the 50 hallmark pathways (rows) that were significantly enriched for DCs of each cDC cluster (columns). (G) Pseudotime trajectory analysis of cDCs with high variable genes. Each dot represents one single cell, colored according to its cluster label. (H) The inlet plot showed each cell with a pseudotime score from dark blue to yellow, indicating early and terminal states, respectively. Gene Set Variation Analysis (I) and violin plots (J) show that cDC_C3 upregulates positive regulation of tolerance induction. (K) Immunohistochemistry revealed differences in LAMP3 expression between two groups (200 µm). Samples with high cDC_C3 scores have a poor prognosis (L) and later clinical stages in the TCGA-THCA cohort (M). cDC, conventional DC; DCs, dendritic cells; OS, overall survival; UMAP, uniform manifold approximation and projection; NES, normalized enrichment score; LAMP3, lysosomal associated membrane protein 3.

LAMP3$^+$ DCs demonstrated upregulation in several pathways, including nuclear factor-kappa B (NF-κB), apoptosis, MAPK signaling, and transcriptional misregulation in cancer, when compared with the other two clusters (figure 4F). Flow cytometry revealed that there was no significant difference in the expression of co-stimulatory molecule (CD80) in LAMP3$^+$ DCs compared with conventional functional DCs; the expression of interleukin (IL)-12, a secret protein that stimulates Th1 cell differentiation, is reduced in LAMP3$^+$ DCs (online supplemental figure S4G,H). These observations indicate that LAMP3$^+$ DCs can be identified as a subset of regulatory and tolerogenic DCs that possess the ability to suppress T-cell activation. We performed pseudotime trajectory analysis, revealing that cDC_C2 cells branched into cDC_C1 cells and LAMP3$^+$ DCs, with LAMP3$^+$ DCs exhibiting the highest pseudotime score, signifying their advanced differentiation and maturation (figure 4G,H). In contrast to other cDC clusters, LAMP3$^+$ DCs displayed upregulation of genes associated with immune tolerance induction, suggesting its pivotal role in the PTC ecosystem (figure 4I,J, online supplemental figure S4B,C). Immunohistochemistry of tissue samples from non-progressive PTC and progressive PTC confirmed the presence of LAMP3$^+$ DCs. Consistent with single-cell findings, a higher proportion of LAMP3 infiltration was observed in progressive PTC cases (figure 4K).

We explored their clinical implications after identifying a specific subset of relevant DCs; the LAMP3$^+$ DC signature was developed using the hypervariable genes specific to LAMP3$^+$ DC. In line with the findings from our scRNA-seq data set, analysis of the TCGA-thyroid carcinoma (THCA) cohort showed significantly higher LAMP3$^+$ DC signature scores in stage T3-T4 PTCs compared with T1-T2. Moreover, higher LAMP3$^+$ DC signature scores in the TCGA-THCA cohort were found to be significantly associated with reduced overall survival (figure 4L,M). These combined results indicated a shift towards increased immunosuppression of DCs in progressive PTC and the LAMP3$^+$ DC is associated with poor prognosis.

Spatial transcriptomics reveals heterogeneity of progressive PTC tumors

Using CellTrek to align single-cell data with spatial transcriptomics slices, more specifically, mapping the single-cell data of A1 and B7 to the spatial transcriptome sequencing of A1 and B7 (SPT-A1, SPT-B7), respectively, we observed notable changes in progressive PTC. There was a significant increase in thyrocytes and fibroblasts, a decrease in the proportion of T and B-cell infiltration, and a greater average distance from tumor cells (figure 5A,B). These findings suggest that progressive PTC tumors pose a greater challenge in eliciting antitumor immune responses. After performing dimensionality reduction and clustering on spatial sequencing data, we found that cluster 9 had a significantly higher three times a day score compared with other cluster spots (figure 5C). Mapping thyrocytes in single-cell data to spatial slices revealed a significant overlap in position between C2_TFF3 and cluster 9. Of particular interest is cluster 8, located in the lower-left corner of the SPT-B7 slice. This cluster shows increased infiltration of T/NK cells but has the lowest three times a day score. At the same time, the tumor cell cluster C6_S100A2, which promotes tumor progression, exhibits significant infiltrations and expansion in this area. The pathological examination shows an increased presence of stroma in this area, with tumor cells displaying outward migration and growth tendencies (figure 5D,E). Using CellTrek to map CD8_C3 and Tregs onto spatial slices, it becomes evident that although CD8_C3 also infiltrates the tumor periphery in non-progressive PTC, the proportion of infiltration is much lower compared with progressive PTC (figure 5F). Tregs were almost undetectable in non-progressive PTC, while in progressive PTC, Tregs infiltration is relatively abundant (figure 5G). Moreover, the spatial distribution of CD8_C3 and Treg cells is relatively consistent in progressive PTC, indicating their synergistic role in promoting tumor immune evasion (figure 5G). Mapping LAMP3$^+$ DC to spatial slices reveals its concentration in the tumor, with progressive PTC exhibiting a higher enrichment ratio that closely overlaps with the spatial distribution of T cells. This suggests a closer interaction between LAMP3$^+$ DC and T cells in progressive PTC (figure 5H). In addition, spatial transcriptomics analysis showed higher immune tolerance scores in progressive PTC, with spots exhibiting higher tolerance scores aligning with T-cell distribution (figure 5I). These findings collectively point to a region where tumor cells, immunosuppressive T-cell subsets, and LAMP3+DC coexist during the progression of PTC, possibly involving complex intercellular interactions that promote the clinical progression of PTC.

Interaction between LAMP3$^+$ DCs and T-cell subpopulations contribute to the formation of an immunosuppressive microenvironment in progressive PTC

Given the consistent trend in progressive PTC for immunosuppressive phenotypes observed in thyrocytes, DCs, and T cells, we hypothesized complex intercellular interactions among different cell populations. Thus, our first objective was to investigate potential intercellular interactions contributing to immunosuppression. Consequently, we found extensive cellular interactions involving LAMP3$^+$ DCs, Treg cells, and CD8$^+$ T cells, facilitated by inhibitory (NECTIN2-TIGIT, LAG3-HAVCR2) or costimulatory (ICOSL-ICOS and CD80/86-CD28) molecules, and chemokines (CXCL16-CXCR6 and CCL17-CCR4) (figure 6A). Treg cells showed elevated CTLA-4 expression, indicating potential interactions with CD80/CD86 molecules in LAMP3$^+$ DCs. This suggests a potential association between Treg and LAMP3$^+$ DCs through ligand-receptor binding. LAMP3$^+$ DCs recruited Treg cells by secreting various chemokines including CCL17-CCR4, CCL5-CCR4, and CCL22-CCR4, and widely activated and enhanced the immunosuppressive function of Treg cells through interactions related to costimulatory signals

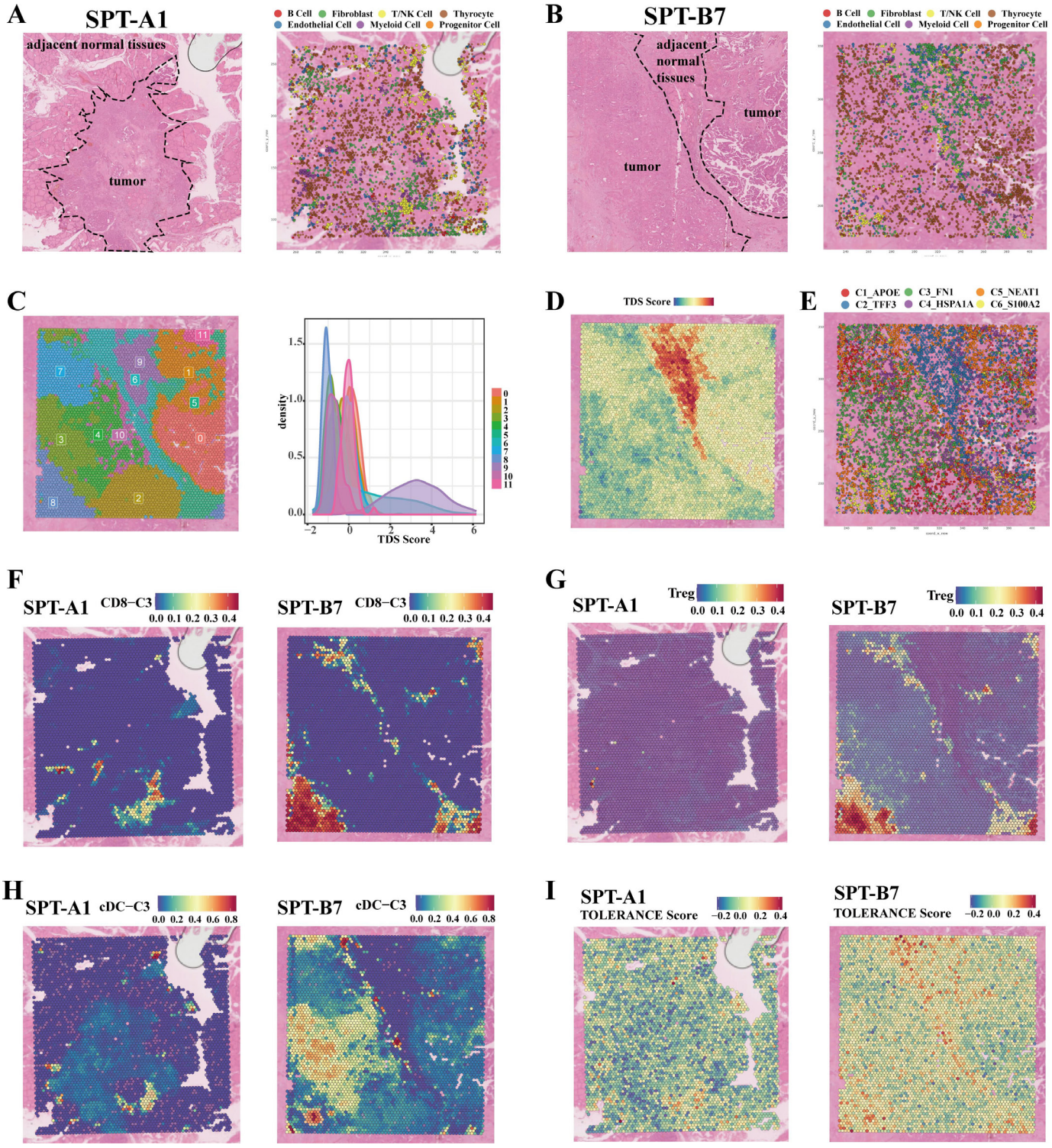

Figure 5 Spatial transcriptomics reveals heterogeneity of progressive papillary thyroid cancer tumors. (A–B) Perform spatial transcriptome sequencing on two paraffin-embedded sample sections and combine them with single-cell sequencing data through CellTrek. (C) Perform dimensionality reduction clustering on the transcriptome data of SPT-B7 and evaluate each cluster of spots using three times a day score. (D) Display the three times a day score of each spot specifically on the slice. (E) Map the six clusters of epithelial cells identified by single-cell sequencing onto the slice. (F–H) Distribution of CD8-C3, Treg, and cDC-C3 cells on slices. (F–H). cDC, conventional dendritic cell; NK, natural killer; Treg, regulatory T cell.

(CD80/CD86-CD28 and ICOSLG-ICOS) and immune evasion (CD86-CTLA-4, NECTIN2-TIGIT, and LGALS9-HAVCR2). We assessed receptor-ligand pairs and found a positive correlation between the abundance of $CD8^+$ T cells and the expression of $LAMP3^+$ DC-secreted chemokines (CXCL16-CXCR6, CXCL10-CXCR3, and CXCL9-CXCR3). $LAMP3^+$ DCs may potentially facilitate the chemotaxis of $CD8^+$ T cells. Compared with

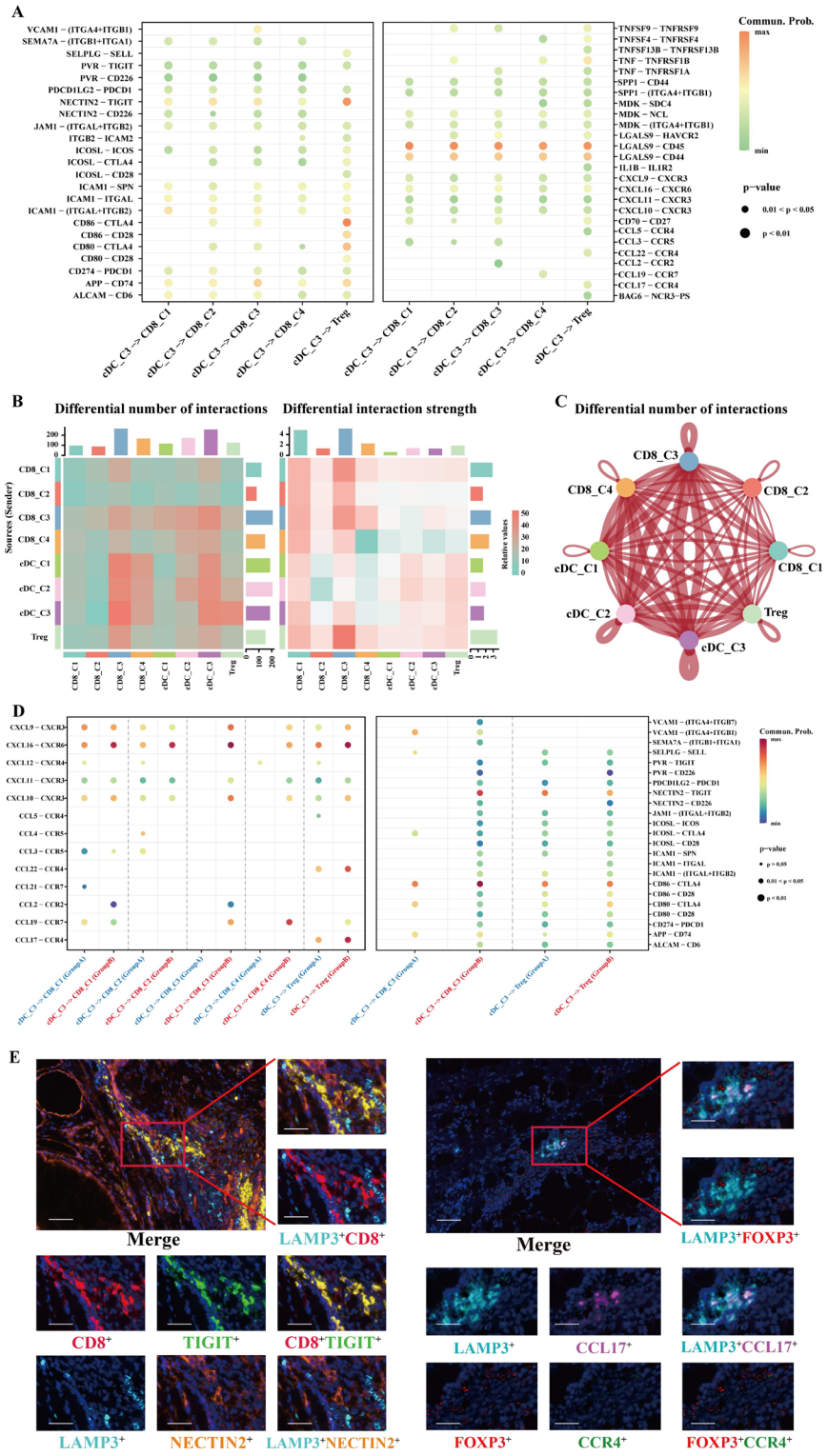

Figure 6 Interaction between LAMP3$^+$ DCs and T-cell subpopulations contribute to the formation of an immunosuppressive microenvironment in progressive PTC. (A) Summary of selected ligand-receptor interactions between the LAMP3$^+$ DCs, CD8$^+$ T cells, and Tregs. Circle size indicates the p value (permutation test). The color gradient represents the interaction strength. Heatmaps (B) and circle (C) plots show the comparison of interaction quantity and interaction strength between LAMP3$^+$ DCs cells, CD8$^+$ T cells, and Tregs between non-progressive PTC and progressive PTC. Red indicated that the increase of communication in the latter. (D) Comparison of the differences in specific cell communication intensity between non-progressive PTC and progressive PTC. (E) Representative immunofluorescence images illustrating the interaction between LAMP3$^+$ DCs and CD8$^+$ T cells or LAMP3$^+$ DCs and Treg cells in one progressive PTC sample (B9). The small panels show the magnification of the selected region highlighted in red. Scale bars correspond to 50 µm in the large panel. CCL17, chemokine (C-C motif) ligand 17;CCR4, chemokine (C-C motif) Receptor 4; cDC. conventional DC; DC, dendritic cell; LAMP3, lysosomal associated membrane protein 3; PTC, papillary thyroid cancer; Treg, regulatory T cell.

non-progressive PTC, we observed a stronger interaction of LAMP3$^+$ DCs with CD8$^+$ T and Treg cells within the TME of cases showing progressive PTC (figure 6B,C, online supplemental figure S5A,B). We also identified a more robust LAMP3$^+$ DC-CD8$^+$ T-cell interaction mediated by CXCL16 and its receptor CXCR6 (figure 6D), essential for recruiting T cells to tumors.[37] This association was validated in the TCGA-THCA cohort, wherein the advanced TNM stage in PTC exhibited significantly elevated levels of CXCL16 (online supplemental figure S5C–E). We delved into the mechanism underlying the exhaustion of recruited CD8$^+$ T cells. In progressive PTC, LAMP3$^+$DCs showed enhanced LGALS9-HAVCR2 and SPP1-CD44 interactions with CD8$^+$ T cells (figure 6D), known to suppress T-cell functions.[35 38 39] Furthermore, LAMP3$^+$ DCs were express PDCD1LG2, CD274, NECTIN2, CD80, and CD86, which are immune checkpoints targeting CTLA-4, TIGIT, and PDCD1,[9 40] thus inhibiting CD8$^+$ T-cell activation (figure 6D). In progressive PTC, the exhausted CD8$^+$ T-cell population (CD8_C3) exhibited intense signaling along with LAMP3$^+$ DCs (figure 6D). Through multiplex immunofluorescence staining, we observed the colocalization of LAMP3-expressing DCs (identified by NECTIN2$^+$) and CD8-expressing CD8$^+$ T cells (identified by TIGIT$^+$) in progressive PTC (figure 6E), which indicated the potential role of LAMP3$^+$ DCs in inducing exhaustion in the recruitment of CD8$^+$ T cells in progressive PTC. We confirmed the recruitment of LAMP3$^+$ DCs (CCL17) on FOXP3_Treg (CCR4) using multiplex fluorescence assay in tissue specimens (figure 6E). Extensive interactions between LAMP3$^+$ DCs and T cells in PTC were found, suggesting that LAMP3$^+$ DCs and T cells work together to shape the immunosuppressive microenvironment in progressive PTC, characterized by high infiltration of exhausted T cells and Treg cells.

The recruitment of LAMP3$^+$ DCs by tumor cells promotes PTC clinical progression

The dynamic interplay between LAMP3$^+$ DCs and T cells accounts for the heightened immune suppression in progressive PTC. However, the interaction between progressive thyroid tumor cells and DCs remains elusive. In order to delve deeper into the specific mechanisms behind the upregulation of LAMP3$^+$ DCs in the progression of PTC, we conducted an analysis of the interactions between tumor cells and LAMP3$^+$ DCs. We observed that the interactions between DCs and epithelial cells were significantly more pronounced in progressive PTC than in non-progressive PTC, indicating a heightened complexity of cellular crosstalk within the TME of progressive PTC (figure 7A–C, online supplemental figure S5F,G). Intercellular adhesion molecule 1, a cell-surface glycoprotein and adhesion receptor responsible for regulating the recruitment of white blood cells to inflammatory sites, exhibited increased interaction with its associated receptors (such as sialophorin or members of the integrin family) in non-progressive PTC[41] (online supplemental figure S5H). Thyroid cells primarily acted as signal senders, and cDC_C1 and cDC_C2 served as signal recipients. cDC_C1 and cDC_C2 serve crucial roles as antigen-presenting cells for activating and assisting CD8$^+$ and CD4$^+$ T cells in their antitumor functions. Group A tumor cells display a more substantial recruitment effect on these cell types. Conversely, when LAMP3$^+$ DCs acted as the signal recipient, Group B tumor cells demonstrated a significantly enhanced recruitment effect on LAMP3$^+$ DCs (figure 7D). Furthermore, the interaction mediated by NECTIN3-NECTIN2, known to promote lymphocyte transendothelial migration, was notably strengthened between tumor cells and LAMP3$^+$ DCs in this context[42] (figure 7E,F). This finding suggests that Group B tumor cells have a greater tendency to recruit LAMP3$^+$ DCs conducive to establishing an immunosuppressive microenvironment. Transcriptomics data from the TCGA database confirmed that the characteristic gene LAMP3 of LAMP3$^+$ DCs positively correlated with the infiltration of CD8$^+$ T cells (CD8A) and Treg cells (FOXP3). Furthermore, the expression level of LAMP3 positively correlated with the T-cell exhaustion marker TIGIT and the expression of the chemokine receptor CCR4, validating our previous findings (online supplemental figure S5I–L).

Subsequently, we performed multiplex fluorescence staining using samples from non-progressive PTC and progressive PTC to validate our analysis results (figure 7G, online supplemental file 7). In Group B tumors, LAMP3$^+$ DCs closely neighbored KRT19$^+$ tumor cells, with a high degree of colocalization of LAMP3 with NECTIN2, KRT19, and NECTIN3, respectively, in sequence. In contrast, in Group A tumors, LAMP3$^+$ DCs were more distant from KRT19$^+$ tumor cells, and NECTIN2 was also expressed on other cell surfaces (such as tumor cells). In Group A, the colocalization of KRT19 with NECTIN3 was insignificant, aligning with our single-cell analysis results. The low expression level of NECTIN3 in non-progressive PTC tumor cells suggested that these tumor cells struggled to retain DCs in the TME through adhesive interaction mediated by NECTIN3-NECTIN2 (figure 7H). In general, the recruitment of LAMP3$^+$ DCs by tumor cells through NECTIN3-NECTIN2 promotes CD8$^+$ T-cell exhaustion and Treg cell infiltration, creating an immunosuppressive microenvironment. This ultimately leads to the clinical progression of PTC.

DISCUSSION

The incidence of PTC is increasing annually.[43] While the overall prognosis of patients is favorable, a subset of cases of PTC displays clinical progression, affecting clinical outcomes. This indicates that cancer is a dynamic disease.[44] Immunotherapy is a promising treatment strategy for patients with unresectable or metastatic tumors.[45] Antibodies targeting cytotoxic T-lymphocyte associated protein 4 (CTLA-4) and programmed cell death 1 (PD-1) and its ligand PD-L1 (CD274 molecule) are the most consolidated options. However, not all patients with the same or different histology experience

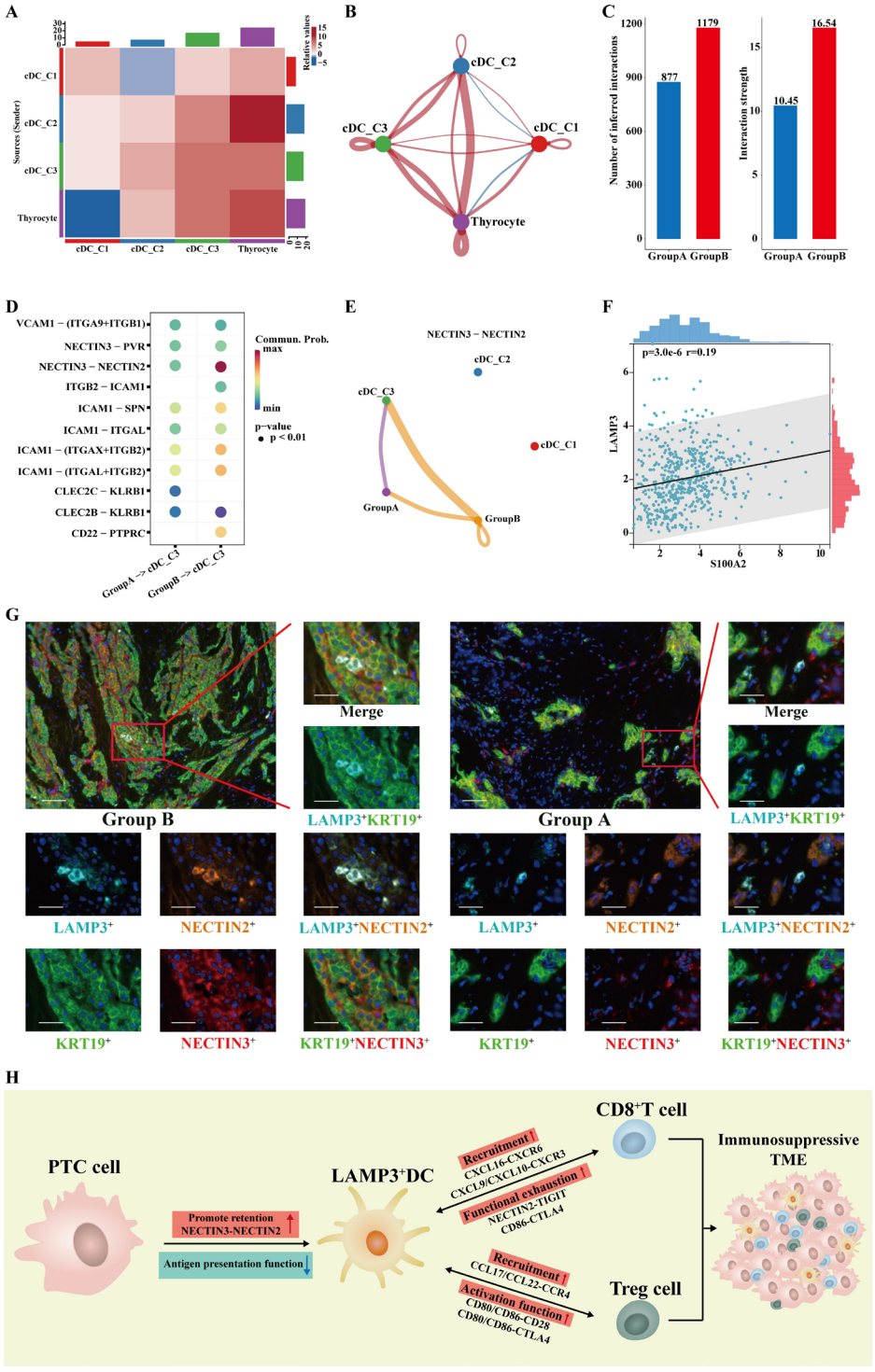

Figure 7 The recruitment of LAMP3$^+$ DCs by tumor cells promotes PTC clinical progression. Heatmaps (A) and circle (B) plots show the comparison of interaction quantity and interaction strength between thyrocytes and cDCs between non-progressive PTC and progressive PTC. Red indicated that the increase of communication in the latter. (C) The interaction between thyrocytes and cDCs is more numerous and stronger in Group B. (D) Summary of selected ligand-receptor interactions between thyrocytes and cDC-C3 cells in the two groups. (E) Circle plots showing the interaction between NECTIN3-NECTIN2 ligand-receptor pairs in the cDCs and thyrocytes. (F) The expression level of S100A2 is positively correlated with LAMP3. (G) Representative immunofluorescence images illustrating the interaction between thyrocytes and cDC_C3 in two groups (A1 and B9). The small panels show the magnification of the selected region highlighted in red. Scale bars correspond to 50 µm in the large panel. (H) Schematic showing the crosstalk among thyrocytes, LAMP3$^+$ DCs, CD8$^+$ T cells, and Tregs involved in the recruitment of immune cells and the formation of an immunosuppressive microenvironment in the progressive PTC. cDC. conventional DC; DC, dendritic cell; CTLA-4, cytotoxic T-lymphocyte associated protein 4; ICAM, intercellular adhesion molecule 1; LAMP3, lysosomal associated membrane protein 3; PTC, papillary thyroid cancer; SPN, sialophorin; TME, tumor microenvironment; Treg, regulatory T cell.

the same benefit.[46–48] Therefore, finding new therapeutic targets is crucial for targeted therapy and immunotherapy of patients with progressive PTC.

In this study, we conducted single-cell sequencing analysis of adjacent normal tissues, non-progressive PTC, and progressive PTC specimens (including cases showing increased tumor diameter, LNM, ETE, and distant metastasis). Our goal was to explore the immune evasion mechanisms underlying the clinical progression of PTC and identify immunotherapy targets. The immune system's response to cancer occurs in three distinct phases: elimination, equilibrium, and escape.[49] During the escape phase, tumors develop multiple mechanisms to reduce antigen presentation and evade immune recognition, including suppression of DC function, and downregulation of human leukocyte antigens-I (HLA-I) expression by interfering with the machinery regulating antigen processing and presentation.[50 51] Emerging and evolved neoplastic cell variants can escape the immune system, leading to tumor growth and clinically evident disease. An in-depth understanding of the TME of PTC and its complex interaction with the immune system is required to leverage the natural immune response and restore the elimination ability of thyroid tumor cells. In our study, we found that the overall presence of immune cells in the TME of progressive PTC was significantly lower compared with the adjacent tissues and non-progressive PTC specimens. Progressive thyrocytes showed higher immune evasion scores. Analysis of immune activity-related genes revealed that most tumor cells exhibit dysfunction in antigen presentation. PTC may show clinical progression by escaping the killing effect of the immune system.

$CD8^+$ T cells possess potent cytotoxicity and are the primary executors of antitumor immune functions.[52] In this study, we observed a substantial infiltration of $CD8^+$ T cells in PTC. However, compared with non-progressive PTC, $CD8^+$ T cell-infiltrating progressive PTC cases exhibit heightened functional exhaustion. Dysregulation of $CD8^+$ T cells in response to tumor antigen stimulation was found. Treg cells, which are immunosuppressive, are recruited to tumors, thereby assisting tumor cells in evading an immune attack by suppressing effector T cells.[53] Furthermore, our study observed an increase in the proportion of infiltrating Treg cells with the onset of clinical progression of PTC. Our finding indicates that immunosuppressive TME is formed in progressive PTC, making tumor cells more prone to immune evasion. However, the specific mechanisms leading to $CD8^+$ T-cell exhaustion and Treg activation warrant further investigations.

DCs play a pivotal role in the antitumor immune processes, wherein alterations in their functionality determine whether cytotoxic events are initiated within the TME, ultimately affecting the suppression of tumor growth.[54–56] However, in recent years, the carcinogenesis of DCs has been gradually uncovered and confirmed. Wang *et al* classified cDC2 into three subpopulations by single-cell sequencing, showing an upregulation of angiogenic capabilities in one subpopulation.[57] Zhang *et al* demonstrated heterogeneity in cDC2, with two tumor-enriched clusters, namely cDC3 and cDC2-TIMP1, exhibiting differential abundances in primary and metastatic tumors.[58] Zhang *et al*'s single-cell study found that $LAMP3^+$ DCs may interact with CD56dimCD16hi NK cells through NECTIN2-TIGIT and IL-15-IL-15R, and NK cells near $LAMP3^+$ DCs express lower levels of granzyme B.[59] In our study, progressive PTC thyrocytes upregulated many functions related to myeloid leukocyte migration and DC chemotaxis. As potent APCs, DCs and the activation and regulation of T cells are closely related. Therefore, we speculated that DCs in progressive PTC may evolve to promote cancer progression. Our study identified a subset of $LAMP3^+$ DCs distinct from cDC1 and cDC2, showing enhanced expression of immune checkpoint-related genes, including CD274 and LGALS9. $LAMP3^+$ DCs are correlated with the advanced T stage and were positively associated with poor prognosis of patients with PTC. Mechanistically, DCs can exert both pro-cancerous and anti-cancerous effects by modulating the T-cell function.[60–63] Therefore, we hypothesized that DCs may exert carcinogenesis by affecting the T-cell function in the clinical progression of PTC. LGALS9-HAVCR2 promotes $CD8^+$ T-cell exhaustion and contributes to the progression of breast cancer, hepatocellular cancer, and glioblastoma.[64–66] Wienke *et al* showed that NECTIN2-TIGIT may regulate T-cell function in neuroblastoma and is a promising target for therapeutic intervention. Combined blockade of TIGIT and PD-L1 significantly reduces neuroblastoma growth, showing complete responses in vivo.[67] Blocking CCR4 can reduce Treg infiltration in bladder cancer, and CCL17 levels in the TME are associated with pituitary adenoma invasiveness and clinical prognosis.[68 69] However, no studies on these receptor-ligand pairs in thyroid cancer have been reported. Our findings indicated that, on the one hand, $LAMP3^+$ DCs promote $CD8^+$ T-cell functional exhaustion through NECTIN2-TIGIT and LGALS9-HAVCR2 interactions. On the other hand, $LAMP3^+$ DCs recruit Treg cells through the secretion of the chemokine, CCL17. Both mechanisms collectively contribute to immune suppression, resulting in the clinical progression of PTC.

Several studies suggested that tumor cells could establish a microenvironment conducive to their growth through cellular interactions.[65 70–73] However, the relationship between tumor cells and DCs remains unclear. We investigated the interaction between tumor cells and $LAMP3^+$ DCs to elucidate the potential mechanism underlying upregulated $LAMP3^+$ DC infiltration during the clinical progression of PTC. Colocalizing tumor cells and NECTIN3 indicates the clinical progression of the tumor. A significant upregulation of NECTIN3 in tumor cells, which are adhesion molecules of the adherens junctions, retained $LAMP3^+$ DCs within the tumor foci by binding to the NECTIN3-NECTIN2. This retention promoted $LAMP3^+$ DCs to exert immunosuppressive functions within the TME by exhausting $CD8^+$ T cells and increasing Treg infiltration, facilitating evasion of immune surveillance by tumor cells.

CONCLUSION

In summary, the present results revealed the dynamic nature of the immune microenvironment in the PTC during disease progression from non-progressive PTC to progressive PTC by demonstrating the key roles of specific immune subpopulations, including LAMP3$^+$ DC, Treg, and exhausted CD8$^+$ T cells. Moreover, we elucidated the specific mechanism by which LAMP3$^+$ DCs mediate immune evasion during PTC clinical progression. These findings may offer new and effective ideas and strategies for immunotherapy in patients with progressive PTC.

Contributors WS and WZ designed the study. ZW, FY and XJ analyzed and interpreted the data. ZW, WZ, ZL, HZ, FY and HS collected clinical samples. ZW and XJ conducted the experiments. ZW, YZ and WS wrote the manuscript. WS, YZ and HZ edited the manuscript. YZ, WS, WZ, ZL, and HZ reviewed the final manuscript. All authors read and approved the final manuscript. WS is the guarantor for the overall content.

Funding This work was supported by the National Natural Science Foundation of China (81902726), Science and Technology Project of Shenyang City (21-173-9-31), Applied Basic Research Program of Liaoning Province (2022020225-JH2/1013), Natural Science Foundation of Liaoning Province (2020-ZLLH-34), National Natural Science Foundation of China (No. 82073244).

Competing interests None declared.

Patient consent for publication Not applicable.

Ethics approval All the procedures involved human subjects were in accordance with the Research Ethics Committee of The First Hospital of China Medical University's (AF-SOP-07-1.1-01) ethical standards. Participants gave informed consent to participate in the study before taking part.

Provenance and peer review Not commissioned; externally peer reviewed.

Data availability statement Data are available upon reasonable request. The data sets (HRA005594) generated and analyzed during the current study are available in the Genome Sequence Archive (GSA) repository, (https://ngdc.cncb.ac.cn/gsa-human/). The data sets used and analyzed during the current study are available from the corresponding author on reasonable request.

ORCID iD

Wei Sun http://orcid.org/0000-0003-1952-128X

REFERENCES

1 Zhang P, Guan H, Yuan S, *et al*. Targeting myeloid derived suppressor cells reverts immune suppression and sensitizes BRAF-mutant papillary thyroid cancer to MAPK inhibitors. *Nat Commun* 2022;13:1588.
2 Pellegriti G, Frasca F, Regalbuto C, *et al*. Worldwide increasing incidence of thyroid cancer: update on epidemiology and risk factors. *J Cancer Epidemiol* 2013;2013:965212.
3 Hadoux J, Pacini F, Tuttle RM, *et al*. Management of advanced medullary thyroid cancer. *Lancet Diabetes Endocrinol* 2016;4:64–71.
4 Naoum GE, Morkos M, Kim B, *et al*. Novel targeted therapies and Immunotherapy for advanced thyroid cancers. *Mol Cancer* 2018;17:51.
5 Bikas A, Vachhani S, Jensen K, *et al*. Targeted therapies in thyroid cancer: an extensive review of the literature. *Expert Rev Clin Pharmacol* 2016;9:1299–313.
6 Widakowich C, de Castro G, de Azambuja E, *et al*. Review: side effects of approved molecular targeted therapies in solid cancers. *Oncologist* 2007;12:1443–55.
7 Ryder M, Gild M, Hohl TM, *et al*. Genetic and pharmacological targeting of CSF-1/CSF-1R inhibits tumor-associated macrophages and impairs BRAF-induced thyroid cancer progression. *PLoS One* 2013;8:e54302.
8 Wang X. Cancer Moonshot 2020: a new March of clinical and translational medicine. *Clin Transl Med* 2016;5:11.
9 Topalian SL, Taube JM, Anders RA, *et al*. Mechanism-driven biomarkers to guide immune checkpoint blockade in cancer therapy. *Nat Rev Cancer* 2016;16:275–87.
10 Stift A, Sachet M, Yagubian R, *et al*. Dendritic cell vaccination in medullary thyroid carcinoma. *Clin Cancer Res* 2004;10:2944–53.
11 Oh D-Y, Algazi A, Capdevila J, *et al*. Efficacy and safety of pembrolizumab monotherapy in patients with advanced thyroid cancer in the phase 2 KEYNOTE-158 study. *Cancer* 2023;129:1195–204.
12 Altorki NK, Markowitz GJ, Gao D, *et al*. The lung microenvironment: an important regulator of tumour growth and metastasis. *Nat Rev Cancer* 2019;19:9–31.
13 Severson JJ, Serracino HS, Mateescu V, *et al*. PD-1+Tim-3+ CD8+ T lymphocytes display varied degrees of functional exhaustion in patients with regionally metastatic differentiated thyroid cancer. *Cancer Immunol Res* 2015;3:620–30.
14 Zhao S, Mi Y, Guan B, *et al*. Tumor-derived Exosomal miR-934 induces macrophage M2 polarization to promote liver metastasis of colorectal cancer. *J Hematol Oncol* 2020;13:156.
15 Liu T, Liu C, Yan M, *et al*. Single cell profiling of primary and paired metastatic lymph node tumors in breast cancer patients. *Nat Commun* 2022;13:6823.
16 Peng W-S, Zhou X, Yan W-B, *et al*. Dissecting the heterogeneity of the microenvironment in primary and recurrent nasopharyngeal carcinomas using single-cell RNA sequencing. *Oncoimmunology* 2022;11:2026583.
17 Gattinoni L, Lugli E, Ji Y, *et al*. A human memory T cell subset with stem cell-like properties. *Nat Med* 2011;17:1290–7.
18 Ohkura N, Sakaguchi S. Transcriptional and epigenetic basis of Treg cell development and function: its genetic anomalies or variations in autoimmune diseases. *Cell Res* 2020;30:465–74.
19 Jiang VC, Hao D, Jain P, *et al*. TIGIT is the central player in T-cell suppression associated with CAR T-cell relapse in Mantle cell lymphoma. *Mol Cancer* 2022;21:185.
20 Mogilenko DA, Shpynov O, Andhey PS, *et al*. Comprehensive profiling of an aging immune system reveals clonal GZMK+ CD8+ T cells as conserved hallmark of inflammaging. *Immunity* 2021;54:99–115.
21 Villani A-C, Satija R, Reynolds G, *et al*. Single-cell RNA-Seq reveals new types of human blood dendritic cells, monocytes, and progenitors. *Science* 2017;356.
22 Guo C, You Z, Shi H, *et al*. SLC38A2 and glutamine signalling in cDC1s dictate anti-tumour immunity. *Nature* 2023;620:200–8.
23 Murphy TL, Murphy KM. Dendritic cells in cancer immunology. *Cell Mol Immunol* 2022;19:3–13.
24 Zhang Q, He Y, Luo N, *et al*. Landscape and dynamics of single immune cells in hepatocellular carcinoma. *Cell* 2019;179:829–45.
25 Zilionis R, Engblom C, Pfirschke C, *et al*. Single-cell transcriptomics of human and mouse lung cancers reveals conserved myeloid populations across individuals and species. *Immunity* 2019;50:1317–34.
26 Lupancu TJ, Eivazitork M, Hamilton JA. CCL17/TARC in autoimmunity and inflammation-not just a T-cell Chemokine. *Immunol Cell Biol* 2023;101:600–9.
27 Ajram L, Begg M, Slack R, *et al*. Internalization of the Chemokine receptor CCR4 can be evoked by orthosteric and allosteric receptor antagonists. *Eur J Pharmacol* 2014;729:75–85.
28 Lin R, Choi YH, Zidar DA, *et al*. B-Arrestin-2-dependent signaling promotes CCR4-mediated Chemotaxis of murine T-helper type 2 cells. *Am J Respir Cell Mol Biol* 2018;58:745–55.
29 Yan Y, Zhao W, Liu W, *et al*. CCL19 enhances CD8+ T-cell responses and accelerates HBV clearance. *J Gastroenterol* 2021;56:769–85.
30 Kurachi M. CD8+ T cell exhaustion. *Semin Immunopathol* 2019;41:327–37.
31 Wherry EJ, Kurachi M. Molecular and cellular insights into T cell exhaustion. *Nat Rev Immunol* 2015;15:486–99.

32 Liu Y, Zhou N, Zhou L, *et al*. IL-2 regulates tumor-reactive CD8+ T cell exhaustion by activating the aryl hydrocarbon receptor. *Nat Immunol* 2021;22:358–69.
33 Nixon BG, Kuo F, Ji L, *et al*. Tumor-associated macrophages expressing the transcription factor IRF8 promote T cell exhaustion in cancer. *Immunity* 2022;55:2044–58.
34 Weisshaar N, Wu J, Ming Y, *et al*. Rgs16 promotes antitumor CD8+ T cell exhaustion. *Science Immunology* 2022;7:eabh1873.
35 Yang R, Sun L, Li C-F, *et al*. Galectin-9 interacts with PD-1 and TIM-3 to regulate T cell death and is a target for cancer immunotherapy. *Nat Commun* 2021;12:832.
36 Rong D, Sun G, Zheng Z, *et al*. MGP promotes CD8+ T cell exhaustion by activating the NF-KB pathway leading to liver metastasis of colorectal cancer. *Int J Biol Sci* 2022;18:2345–61.
37 Korbecki J, Bajdak-Rusinek K, Kupnicka P, *et al*. The role of CXCL16 in the pathogenesis of cancer and other diseases. *Int J Mol Sci* 2021;22:3490.
38 Morishita A, Oura K, Tadokoro T, *et al*. Galectin-9 in gastroenterological cancer. *Int J Mol Sci* 2023;24:6174.
39 Klement JD, Paschall AV, Redd PS, *et al*. An Osteopontin/CD44 immune checkpoint controls CD8+ T cell activation and tumor immune evasion. *J Clin Invest* 2018;128:5549–60.
40 Tsai H-F, Hsu P-N. Cancer immunotherapy by targeting immune checkpoints: mechanism of T cell dysfunction in cancer immunity and new therapeutic targets. *J Biomed Sci* 2017;24:35.
41 Bui TM, Wiesolek HL, Sumagin R. ICAM-1: a master regulator of cellular responses in inflammation, injury resolution, and tumorigenesis. *J Leukoc Biol* 2020;108:787–99.
42 Devilard E, Xerri L, Dubreuil P, *et al*. Nectin-3 (CD113) interacts with Nectin-2 (CD112) to promote lymphocyte transendothelial migration. *PLoS One* 2013;8:e77424.
43 Miranda-Filho A, Lortet-Tieulent J, Bray F, *et al*. Thyroid cancer incidence trends by histology in 25 countries: a population-based study. *Lancet Diabetes Endocrinol* 2021;9:225–34.
44 Ardito G, Revelli L, Giustozzi E, *et al*. Aggressive papillary thyroid microcarcinoma: prognostic factors and therapeutic strategy. *Clin Nucl Med* 2013;38:25–8.
45 Waldman AD, Fritz JM, Lenardo MJ. A guide to cancer immunotherapy: from T cell basic science to clinical practice. *Nat Rev Immunol* 2020;20:651–68.
46 Janjigian YY, Shitara K, Moehler M, *et al*. First-line nivolumab plus chemotherapy versus chemotherapy alone for advanced gastric, gastro-oesophageal junction, and oesophageal adenocarcinoma (Checkmate 649): a randomised, open-label, phase 3 trial. *Lancet* 2021;398:27–40.
47 Liu SV, Reck M, Mansfield AS, *et al*. Updated overall survival and PD-L1 subgroup analysis of patients with extensive-stage small-cell lung cancer treated with atezolizumab, carboplatin, and etoposide (Impower133). *J Clin Oncol* 2021;39:619–30.
48 Larkin J, Chiarion-Sileni V, Gonzalez R, *et al*. Five-year survival with combined nivolumab and Ipilimumab in advanced melanoma. *N Engl J Med* 2019;381:1535–46.
49 Dunn GP, Bruce AT, Ikeda H, *et al*. Cancer immunoediting: from immunosurveillance to tumor escape. *Nat Immunol* 2002;3:991–8.
50 Jhunjhunwala S, Hammer C, Delamarre L. Antigen presentation in cancer: insights into tumour immunogenicity and immune evasion. *Nat Rev Cancer* 2021;21:298–312.
51 Hangai S, Ao T, Kimura Y, *et al*. PGE2 induced in and released by dying cells functions as an inhibitory DAMP. *Proc Natl Acad Sci USA* 2016;113:3844–9.
52 Reina-Campos M, Scharping NE, Goldrath AW. CD8+ T cell metabolism in infection and cancer. *Nat Rev Immunol* 2021;21:718–38.
53 Wing JB, Tanaka A, Sakaguchi S. Human FOXP3+ regulatory T cell heterogeneity and function in autoimmunity and cancer. *Immunity* 2019;50:302–16.
54 Wculek SK, Cueto FJ, Mujal AM, *et al*. Dendritic cells in cancer immunology and immunotherapy. *Nat Rev Immunol* 2020;20:7–24.
55 Gardner A, de Mingo Pulido Á, Ruffell B. Dendritic cells and their role in immunotherapy. *Front Immunol* 2020;11:924.
56 Morante-Palacios O, Fondelli F, Ballestar E, *et al*. Tolerogenic dendritic cells in autoimmunity and inflammatory diseases. *Trends Immunol* 2021;42:59–75.
57 Huang X-Z, Pang M-J, Li J-Y, *et al*. Single-cell sequencing of ascites fluid illustrates heterogeneity and therapy-induced evolution during gastric cancer peritoneal metastasis. *Nat Commun* 2023;14:822.
58 Liu Y, Zhang Q, Xing B, *et al*. Immune phenotypic linkage between colorectal cancer and liver metastasis. *Cancer Cell* 2022;40:424–37.
59 Tang F, Li J, Qi L, *et al*. A pan-cancer single-cell panorama of human natural killer cells. *Cell* 2023;186:4235–51.
60 Rodrigue-Gervais IG, Rigsby H, Jouan L, *et al*. Dendritic cell inhibition is connected to exhaustion of CD8+ T cell polyfunctionality during chronic hepatitis C virus infection. *J Immunol* 2010;184:3134–44.
61 Liu J, Zhang S, Hu Y, *et al*. Targeting PD-1 and Tim-3 pathways to reverse CD8 T-cell exhaustion and enhance ex vivo T-cell responses to autologous dendritic/tumor vaccines. *J Immunother* 2016;39:171–80.
62 Hilligan KL, Ronchese F. Antigen presentation by dendritic cells and their instruction of CD4+ T helper cell responses. *Cell Mol Immunol* 2020;17:587–99.
63 Fu C, Jiang A. Dendritic cells and CD8 T cell immunity in tumor microenvironment. *Front Immunol* 2018;9:3059.
64 Yuan F, Cai X, Cong Z, *et al*. Roles of the M6A modification of RNA in the glioblastoma microenvironment as revealed by single-cell analyses. *Front Immunol* 2022;13:798583.
65 Ho DW-H, Tsui Y-M, Chan L-K, *et al*. Single-cell RNA sequencing shows the immunosuppressive landscape and tumor heterogeneity of HBV-associated hepatocellular carcinoma. *Nat Commun* 2021;12:3684.
66 Zou Y, Ye F, Kong Y, *et al*. The single-cell landscape of intratumoral heterogeneity and the immunosuppressive microenvironment in liver and brain metastases of breast cancer. advanced science. *Advanced Science* 2023;10:e2203699.
67 Wienke J, Visser L, Kholosy W, *et al*. Integrative analysis of neuroblastoma by single-cell RNA sequencing identifies the NECTIN2-TIGIT axis as a target for immunotherapy. *Cancer Cell* 2023.
68 Zhang A, Xu Y, Xu H, *et al*. Lactate-induced M2 polarization of tumor-associated macrophages promotes the invasion of pituitary adenoma by secreting CCL17. *Theranostics* 2021;11:3839–52.
69 Zhao H, Bo Q, Wang W, *et al*. CCL17-CCR4 axis promotes metastasis via ERK/MMP13 pathway in bladder cancer. *J Cell Biochem* 2019;120:1979–89.
70 Mao X, Xu J, Wang W, *et al*. Crosstalk between cancer-associated fibroblasts and immune cells in the tumor microenvironment: new findings and future perspectives. *Mol Cancer* 2021;20:131.
71 Bayik D, Lathia JD. Cancer stem cell-immune cell crosstalk in tumour progression. *Nat Rev Cancer* 2021;21:526–36.
72 Jiang H, Yu D, Yang P, *et al*. Revealing the transcriptional heterogeneity of organ-specific metastasis in human gastric cancer using single-cell RNA sequencing. *Clin Transl Med* 2022;12:e730.
73 Baghban R, Roshangar L, Jahanban-Esfahlan R, *et al*. Tumor microenvironment complexity and therapeutic implications at a glance. *Cell Commun Signal* 2020;18:59.